NSS

Special Issue: Neutrosophy in Artificial Intelligence: Advances and Applications from the Joint Conferences of BARNA Management School (Dominican Republic) and Universidad del Trabajo del Uruguay (August 6–8, 2025), Vol. 92, 2025

University of New Mexico

Neutrosophic Statistical Analysis of Temperature and Precipitation Variability over Four Decades in the City of Pucallpa, Peru

Noé Klever Guadalupe-Baylón[1]*, Edgar Juan Diaz-Zúñiga[2], Moisés Amancio Cueva-Muñoz[3], Nadia Masaya Panduro-Tenazoa[4], Noé Ramírez-Flores[5], Franz Orlando Tang-Jara[6] and Carlos Ricardo Guerra-Pinedo[7]

[1] Universidad Nacional de Ucayali, Pucallpa, Ucayali, Perú. noe_guadalupe@unu.edu.pe
[2] Universidad Nacional de Ucayali, Pucallpa, Ucayali, Perú. edgar_diaz@unu.edu.pe
[3] Universidad Nacional de Ucayali, Pucallpa, Ucayali, Perú. moises_cueva@unu.edu.pe
[4] Universidad Nacional Intercultural de la Amazonía, Pucallpa, Ucayali, Perú. nmpandurot@unia.edu.pe
[5] Instituto de Investigaciones de la Amazonía Peruana, Pucallpa, Ucayali, Perú. nramirez@iiap.gob.pe
[6] Gerencia Regional Forestal y de Fauna Silvestre, Pucallpa, Ucayali, Perú. franztangjara@gmail.com
[7] Universidad Nacional de Ucayali, Pucallpa, Ucayali, Perú. carlos_guerra@unu.edu.pe

Abstract. This study analyses the spatiotemporal variation of temperature and rainfall in Pucallpa (1984-2024) and its relationship with El Niño and La Niña phenomena and urban expansion. Monthly meteorological data from the UNU-SENAMHI station, weather, ENSO indices, and Landsat imagery were used to calculate the Normalized Difference Vegetation Index (NDVI) as an indicator of vegetation cover. Missing data were processed through interpolation, and linear regression analysis, the Mann-Kendall test, and Spearman correlation adapted to interval-valued data were applied to evaluate trends and statistical associations. Our findings highlight the combined influence of global climatic factors and local transformations on the microclimate of Pucallpa. To reach our conclusions, we used Neutrosophic Statistics as a study tool. This theory extends classical statistics when there are interval-based data or parameters, or when the population size is imprecise. Neutrosophic Statistics can improve accuracy by capturing the indeterminacies that exist in measurements. This tool allows us to assess changes in temperature and precipitation during the year, which are not homogeneous throughout the region. Specifically, we use intervals of maximum and minimum temperatures during the month.

Keywords: Temperature variability, precipitation variability, Mann-Kendall test, Spearman correlation, ENSO, Neutrosophic Statistics, Neutrosophy.

1. Introduction

Climate change represents one of the greatest challenges to global sustainability, with impacts that vary across geographic and socioeconomic scales. Globally, the increase in average temperature (+1.1 °C since the pre-industrial era) has intensified extreme weather events, disrupted hydrological cycles, and threatened ecosystems. In Peru, a megadiverse and highly vulnerable country, this phenomenon is reflected in the retreat of Andean glaciers (a 53.56% loss in glacier surface over 54 years) and the increasing frequency of El Niño-Southern Oscillation (ENSO) events, which have had significant economic repercussions. Peru's Gross Domestic Product fell by 10% during the 1982-1983 El Niño event, by 0.4% in 1997-1998, and growth was reduced by 1.5% in 2017 due to severe damage from floods and landslides, affecting infrastructure, consumption, and investment. Locally, the city of Pucallpa, located in the Peruvian Amazon, faces rapid urbanization and forest cover loss in its surroundings, conditions that heighten its vulnerability to extreme climate events.

Thermal and rainfall variability in tropical regions is shaped by both natural and anthropogenic factors. ENSO events modulate precipitation patterns in the Amazon, while heat waves and cold snaps (cold air incursions) disrupt historical seasonal patterns. However, accelerated urbanization has emerged as a critical driver: the replacement of vegetation with impervious surfaces increases land surface temperature (urban heat island effect, UHI) and reduces relative humidity. In Pucallpa, this process has been driven by road and agricultural expansion, undermining the regulatory capacity of natural ecosystems.

The relationship between urban expansion and meteorological parameters has been documented through studies linking the growth of built-up areas with thermal anomalies. In cities such as Manaus, Belém, and Huancayo, urban growth has been accompanied by significant increases in mean temperature and its extremes. These findings suggest that forest loss, partly driven by urbanization, not only alters microclimates but also interacts with large-scale phenomena such as Amazonian atmospheric convection and regional climate stability.

Assessing climate trends and their links to anthropogenic variables requires multidisciplinary approaches. Linear and polynomial regression models have been used to quantify rates of temperature change. Non-parametric tests such as the Mann-Kendall test have also been employed to detect significant trends in time series with non-normal distributions, evaluating their statistical power and sensitivity to various factors. To isolate the impact of urbanization, recent studies apply correlation analyses (Pearson and Spearman), controlling for natural variability such as ENSO. Remote sensing, using indices such as NDVI and supervised classifications of Landsat/Sentinel imagery, allows for mapping of urban and vegetation cover changes at resolutions ≤30 m. These tools, validated in contexts such as Manaus, Belém, and Minas Gerais (Brazil), offer a replicable framework for Amazonian cities.

This study aims to analyze the spatiotemporal variation of temperature and precipitation in Pucallpa (1984–2024) and to assess their relationship with El Niño and La Niña events and urban expansion through statistical analyses and remote sensing. Pucallpa, a hub of migration and economic development in the Peruvian Amazon, lacks comprehensive studies that disentangle the climatic effects of urbanization from natural variability. The findings will provide quantitative evidence for territorial planning and climate adaptation policies, prioritizing local scales within global sustainability agendas.

Classical statistical methods are based on measurements taken from spatial points at a specific instant, which are considered representative of much larger regions over longer periods. It is well known that temperatures and precipitation are not uniform; each space within a region experiences changes throughout the day in terms of these two meteorological variables. The most basic aspect is that there are maximum and minimum temperatures during the day. This is why studies of these variables have been conducted based on Neutrosophic Statistics, because incorporating indeterminacy is a way to gain accuracy [1-3].

Neutrosophic Statistics is the extension of classical statistics to the field of neutrosophy. Neutrosophy is the branch of philosophy that studies neutrality, which is the concept that encompasses not only the neutral, but also the unknown, incomplete information, the paradoxical, the inconsistent, the contradictory, the erroneous, and so on [4-6].

Thus, Neutrosophic Statistics is the adaptation of classical statistical methods to situations where data or parameters are in the form of intervals, or when the sample size or population is not precisely defined. In this way, more reliable results can be obtained from the real phenomena being studied, which are often complex [7-11]. In this article, we use this theory to more accurately capture the behavior of precipitation and temperature in the Pucallpa region.

The paper is divided into a Materials and Methods section, which explains the fundamental concepts of Neutrosophic Statistics. Later, the Results section provides the basic details of the study and the results obtained. The final section is the Conclusion.

2. Materials and Methods

In this section, we briefly review the main notions of Neutrosophic Statistics.

Definition 1: ([4, 5]) Given X is a universe of discourse and A is a subset of X. $u_A(x), r_A(x), v_A(x) : X \to \,]^-0, 1^+[$, are three membership functions of truthfulness, indeterminacy and falseness of x in A, respectively, satisfying the constraint $^-0 \leq \inf u_A(x) + \inf r_A(x) + \inf v_A(x) \leq \sup u_A(x) + \sup r_A(x) + \sup v_A(x) \leq 3^+$ for all x∈X. Then A is called a *Neutrosophic Set* (NS) over standard or non-standard subsets of $]^-0, 1^+[$.

Definition 2: ([4, 5]) Given X is a universe of discourse and A is a subset of X, where:

$$A = \{(x, u_A(x), r_A(x), v_A(x)) : x \in X\} \quad (1)$$

Then, A is called a *Single-Valued Neutrosophic Set* (SVNS) on X if it satisfies:

$u_A, r_A, v_A : X \to [0,1]$, and $0 \leq u_A(x) + r_A(x) + v_A(x) \leq 3$ for all x∈X. $u_A(x), r_A(x)$, and $v_A(x)$ represent the membership functions of truthfulness, indeterminacy, and falseness of x in A, respectively. Whereas, a *Single-Valued Neutrosophic Number* (SVNN) is denoted by $A = (a, b, c)$, such that $a, b, c \in [0,1]$ and $0 \leq a + b + c \leq 3$.

- *Neutrosophic Statistics* generalizes classical statistics by incorporating set-valued data instead of crisp values [1]. This framework aligns with the nature of the data analyzed in this study.
- *Neutrosophic Descriptive Statistics* encompasses techniques for summarizing and characterizing neutrosophic numerical data.
- *Neutrosophic Inferential Statistics* includes methods for extrapolating conclusions from neutrosophic samples to their respective populations.

Neutrosophic data contains elements of indeterminacy and can be classified analogously to classical data:

- *Discrete neutrosophic data*: values are isolated points.
- *Continuous neutrosophic data*: values span one or more intervals.
- *Quantitative neutrosophic data*: e.g., uncertain numerical values such as 47, 52, 67, or 69.
- *Qualitative neutrosophic data*: e.g., uncertain categorical values such as blue or red; or white, black, green, or yellow.
- *Univariate neutrosophic data* involves observations on a single neutrosophic attribute.
- *Multivariate neutrosophic data* involves observations on multiple attributes.
- A *Neutrosophic Statistical Number* N is expressed as N=d+I, where *d* is the determinate part and *I* is the indeterminate part.
- A *Neutrosophic Frequency Distribution* presents categories, frequencies, and relative frequencies with indeterminacy, often due to incomplete or imprecise data.
- *Neutrosophic Survey Results* contain elements of indeterminacy.
- A *Neutrosophic Population* is one where membership is not precisely defined.
- A *Simple Random Neutrosophic Sample* of size *n* includes at least one individual with indeterminate characteristics.
- A *Stratified Random Neutrosophic Sample* involves dividing the population into strata and sampling from each of them, with indeterminacy present in at least one stratum.

Let $N_1 = a_1 + b_1 I$ and $N_2 = a_2 + b_2 I$ be neutrosophic numbers. The operations are defined as [1, 2, 12]:

- Addition: $N_1 + N_2 = a_1 + a_2 + (b_1 + b_2)I$,
- Subtraction: $N_1 - N_2 = a_1 - a_2 + (b_1 - b_2)I$,
- Multiplication: $N_1 \times N_2 = a_1 a_2 + (a_1 b_2 + b_1 a_2 + b_1 b_2)I$,
- Division: $\frac{N_1}{N_2} = \frac{a_1 + b_1 I}{a_2 + b_2 I} = \frac{a_1}{a_2} + \frac{a_2 b_1 - a_1 b_2}{a_2(a_2 + b_2)} I$.

For intervals $I_1 = [a_1, b_1]$ and $I_2 = [a_2, b_2]$ [1, 2]:

- $I_1 \leq I_2$ iff $a_1 \leq a_2$ and $b_1 \leq b_2$.
- Addition: $I_1 + I_2 = a_1 + a_2 + (b_1 + b_2)I$,
- Subtraction: $I_1 - I_2 = a_1 - a_2 + (b_1 - b_2)I$,
- Multiplication: $I_1 \cdot I_2 = [\min\{a_1 \cdot b_1, a_1 \cdot b_2, a_2 \cdot b_1, a_2 \cdot b_2\}, \max\{a_1 \cdot b_1, a_1 \cdot b_2, a_2 \cdot b_1, a_2 \cdot b_2\}]$,
- Division: $\frac{I_1}{I_2} = \left[\frac{a_1}{b_1}, \frac{a_2}{b_2}\right]$, provided $0 \notin I_2$,
- Square Root: $\sqrt{I} = \left[\sqrt{a}, \sqrt{b}\right]$, assuming $a \geq 0$,
- Exponentiation: $I^n = \underbrace{I \cdot I \cdot \cdots \cdot I \cdot I}_{n \text{ times}}$.

Definition 3 ([12]) A and B are two single-valued neutrosophic sets in a finite space $X = \{x_1, x_2, \ldots, x_n\}$. One *neutrosophic correlation* between A and B is defined as:

$$CN(A, B) = \sum_{i=1}^{n} [u_A(x_i)u_B(x_i) + r_A(x_i)r_B(x_i) + v_A(x_i)v_B(x_i)] \quad (2)$$

The *correlation coefficient* is given by:

$$R(A, B) = \frac{CN(A,B)}{\sqrt{T(A)T(B)}} \quad (3)$$

Such that:

$T(A) = \sum_{i=1}^{n} [u_A^2(x_i) + r_A^2(x_i) + v_A^2(x_i)]$ and $T(B) = \sum_{i=1}^{n} [u_B^2(x_i) + r_B^2(x_i) + v_B^2(x_i)]$.

3. Results

Within the theory of Neutrosophic Statistics, we will primarily rely on the method described in [13], and see also [14]. The analysis covered 492 months of continuous climate records (1984–2024).

We will define two variables $T_{iN} = [T_{iNL}, T_{iNU}]$, and P_{iN} to denote the temperature and precipitation in the ith month (i=1, 2,…, 492).

T_{iNL} is the minimum temperature of the month measured in degrees Celsius,

T_{iNU} is the maximum temperature of the month measured in degrees Celsius,

P_{iN} is the precipitation during the ith month measured in mm,

Two essential measures are the average temperature and precipitation, which are calculated using Equations 4 and 5, respectively.

$$\bar{T}_N = [\bar{T}_{NL}, \bar{T}_{NU}] \quad (4)$$

$$\bar{P}_N = \frac{\sum_{i=1}^{492} P_{iN}}{492} \quad (5)$$

Where:

$\bar{T}_{NL} = \frac{\sum_{i=1}^{492} T_{iNL}}{492}$,

$\bar{T}_{NU} = \frac{\sum_{i=1}^{492} T_{iNU}}{492}$.

The difference between each temperature value and the average is calculated as follows:

$T_{iN} - \bar{T}_N = [T_{iNL} - \bar{T}_{NL}, T_{iNU} - \bar{T}_{NU}]$,

Also we have:

$(T_{iN} - \bar{T}_N)^2 = ([T_{iNL} - \bar{T}_{NL}, T_{iNU} - \bar{T}_{NU}])^2$,

Where the square of an interval is calculated using the equations presented in the previous section.

The Neutrosophic Standard Deviation for temperature is calculated as:

$\sigma_T = \sqrt{\frac{\sum_{i=1}^{492}(T_{iN}-\bar{T}_N)^2}{492}}$,

The variance is calculated as:

$\sigma_T^2 = \frac{\sum_{i=1}^{492}(T_{iN}-\bar{T}_N)^2}{492}$.

For the STD and variance we have to use the equations of operations over intervals.

The Mann-Kendall test is a non-parametric statistical test used to identify trends in time series data, particularly useful when the data does not follow a normal distribution [15, 16]. It detects monotonic trends, and it checks for consistent upward or downward trends over time. There is no assumption of distribution, unlike parametric tests; it does not require the data to be normally distributed. It is widely used in environmental science, hydrology, climate studies, and other fields dealing with long-term observational data [17].

The null hypothesis is H_0: No trend exists.

The alternative hypothesis is H_1: A trend (positive or negative) exists.

The method consists of:

1. Comparing each data point with all subsequent points.
2. Counts the number of times later values are higher or lower than earlier ones.
3. Calculates a statistic (S) based on these comparisons.
4. Uses a normal approximation (Z-score) for significance testing when the sample size is large.

Important considerations are the following:

- Autocorrelation: The test assumes no serial correlation. If present, it can be bias results.
- Seasonality: For seasonal data, we should use the Seasonal Kendall Test instead.
- Minimum data points: At least 8–10 observations are recommended for reliable results.

For the case of intervals, we use the following adapted statistic:

$S = \sum_{j=1}^{n-1}\sum_{k=j+1}^{n} sign\left([a_k, b_k] - [a_j, b_j]\right)$, where:

$$sign\left([a_k, b_k] - [a_j, b_j]\right) = \begin{cases} +1, if\ a_k > b_j \\ -1,\ if\ b_k < b_j \\ 0, otherwise \end{cases},$$

The remaining steps follow the classic test.

Spearman's coefficient (ϱ) measures the correlation between two variables using their ranges instead of the original values. The classic formula is [18, 19]:

$\rho = 1 - \frac{6\sum_{i=1}^{n} D_i^2}{n(n^2-1)}$,

Where: D_i is the difference between the ranges of each pair of observations, n is the number of observations.

When the data are intervals, with two data series $X_i = [a_i, b_i]$ and $Y_i = [c_i, d_i]$, ranges cannot always be assigned directly. However, the midpoint can be used, that is, each interval is transformed into its midpoint: $x_i = \frac{a_i+b_i}{2}$ and $y_i = \frac{c_i+d_i}{2}$. The classic Spearman test is then applied to the midpoints.

Below, we describe the results obtained, starting with the location of the study area.

This study was conducted in the city of Pucallpa, covering an area of influence defined by a 15 km radius centered at coordinates 8°24′48″ S and 74°34′18″ W, corresponding to the location of the Principal Climatological Station UNU-SENAMHI (Figure 1). This delimitation encompasses urban, peri-urban, and adjacent forested zones, enabling the analysis of interactions between urban expansion and climatic parameters. The radius was selected to capture the spatial influence of urbanization on local microclimates, considering the resolution of satellite imagery (30 m) and the historical distribution of meteorological data.

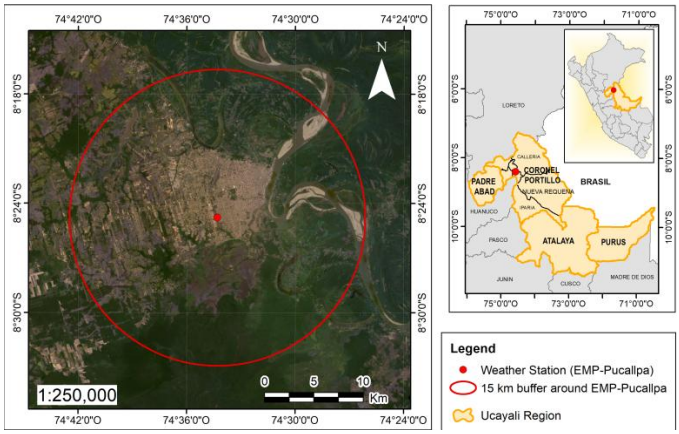

Figure 1. Location of the study area.

The data collection phase was divided into three subcomponents. First, meteorological data were obtained from the EMP-Pucallpa, including monthly averages of maximum, minimum, and mean temperature (°C), as well as accumulated precipitation (mm), for the period 1984–2024 (41 years). Second, El Niño Coastal Index (ICEN) data were compiled from the National Study of the El Niño Phenomenon and SST data from NOAA's Extended Reconstruction Sea Surface Temperature Version 5 (ERSSTv5). Third, satellite imagery from Landsat 5 TM and Landsat 8 OLI was downloaded via the Earth Explorer portal, prioritizing Level-2 processing scenes (with atmospheric correction) and low cloud cover. For each selected year, only scenes with optimal conditions for spectral analysis were used, discarding images with clouds, shadows, or saturation issues.

From these images, the Normalized Difference Vegetation Index (NDVI) was calculated using the formula:

$$NDVI = (NIR - RED) / (NIR + RED) \quad (6)$$

Where NIR represents the near-infrared band and RED the red band.

The spectral bands used were: Landsat 5 TM; Band 3 (RED: 0.63–0.69 μm), Band 4 (NIR: 0.76–0.90 μm), and Landsat 8 OLI; Band 4 (RED: 0.64–0.67 μm), Band 5 (NIR: 0.85–0.88 μm). The calculations were performed in ArcGIS 10.8 using the Raster Calculator tool.

Then, the average NDVI value within a 15 km buffer around the EMP-Pucallpa meteorological station was extracted and considered the urban influence area. This means the NDVI value per scene was interpreted as an indirect indicator of vegetation cover in the study area. NDVI reduction over time was associated with urban expansion processes, based on the assumption that urban growth leads to the loss of natural vegetation, especially in rapidly urbanizing peripheral zones.

To enable monthly correlation analysis between climatic variables and NDVI, missing NDVI values were interpolated using a temporal approximation, generating a continuous monthly series from 1984 to 2024. This interpolated series allowed comparison with the monthly records of temperature and rainfall, facilitating better evaluation of the relationships between vegetation cover changes and climate conditions.

Data processing was carried out in three stages. Initially, missing values in the meteorological time series (≤5% of the total) were addressed using spline interpolation. This technique was selected for its ability to model the continuity of climatic variables while minimizing bias in the analysis. Its application to meteorological data has been validated in studies that demonstrated that cubic splines allow accurate estimation of missing temperature and precipitation data. Subsequently, statistical analysis of the time series and urban expansion was performed. To evaluate temperature and precipitation variability over time, a linear regression model was applied, expressed by the equation:

$$y = mx + b \quad (7)$$

Where "y" represents the dependent variable (climatic variable), "x" denotes time (in years), "m" is the slope of the line, indicating its steepness "b" is the y-intercept (when x = 0).

Figure 2 shows the comparison between the NDVI of Equation 6, between the years 1984 and 2024.

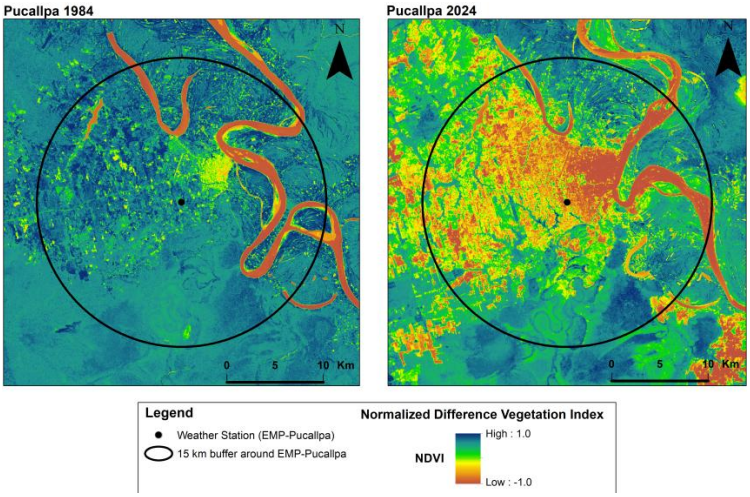

Figure 2. Vegetation Dynamics (NDVI) around Pucallpa Weather Station (UNU-SENAMHI): 1984 vs. 2024.

This pattern reflects landscape transformation consistent with urban expansion processes. Although NDVI does not directly measure urbanization, it allows inference of such processes insofar as urban growth typically involves the replacement of vegetation by built-up or degraded surfaces.

The Mann-Kendall test was applied, adapted to the intervals between the minimums and maximums, as explained at the beginning of this section, and the results were as follows:

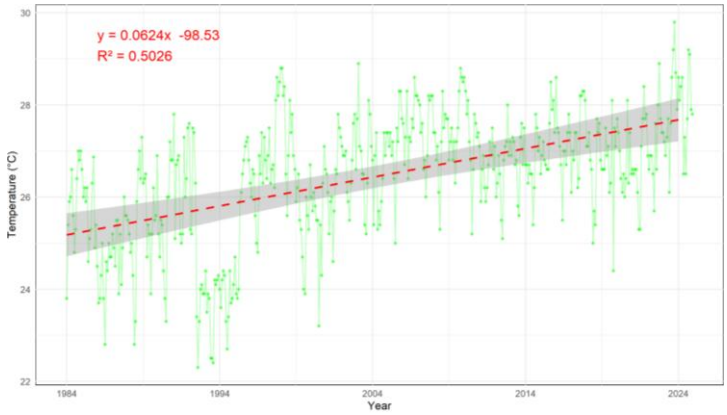

Figure 3. Average temperature time series with annual trend.

Mean temperature exhibited a rising trend as well, modeled by y=0.0624x−98.53, reflecting an annual increase of 0.0624 °C and a cumulative increase of 2.5 °C over 40 years (Figure 3). The coefficient of determination (R^2 = 0.5026) suggests a moderate-to-strong relationship with time. The Mann-Kendall test also confirmed a highly significant trend ($p < 0.05$) with a positive S value (43.502), and a moderate-to-high correlation (Tau = 0.3644), indicating sustained warming throughout the study period.

The same thing happened with the maximum and minimum temperatures. See Figures 4 and 5.

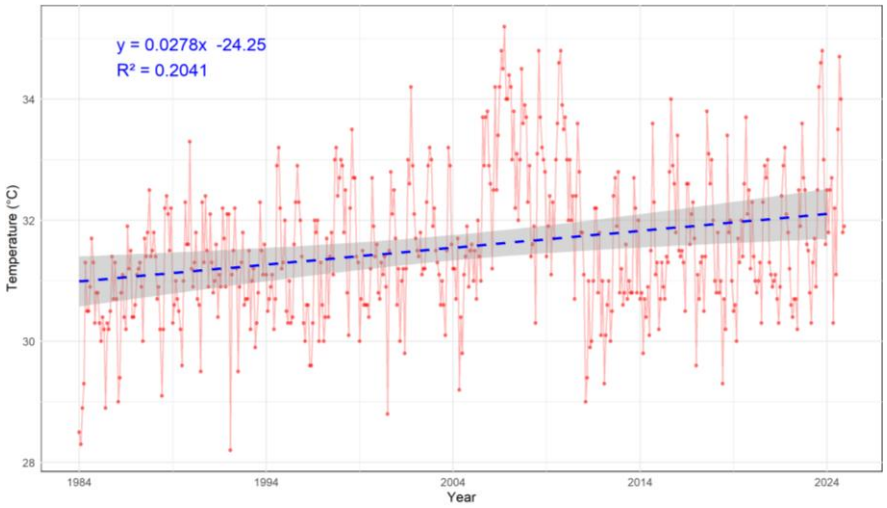

Figure 4. Maximum temperature time series with annual trend.

Maximum temperature shows an upward trend with the regression equation y=0.0278x−24.25, indicating an annual increase of 0.0278 °C, equivalent to a cumulative rise of 1.1 °C over four decades (Figure 4).

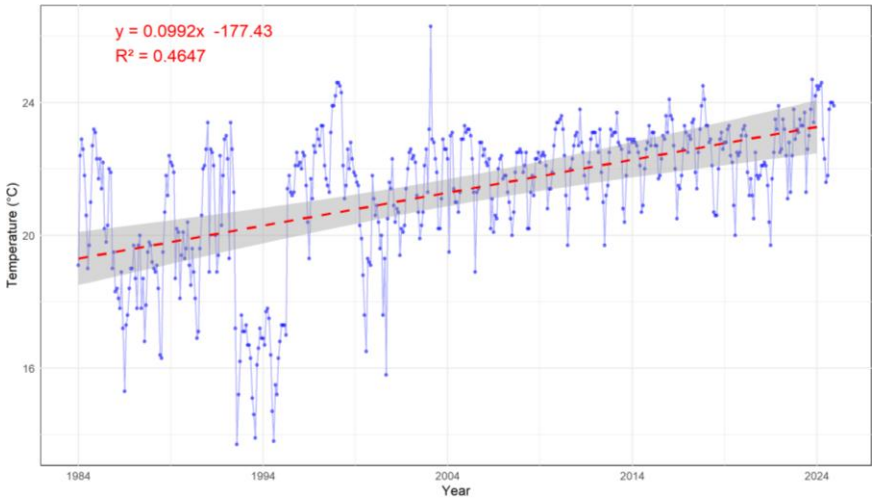

Figure 5. Minimum temperature time series with annual trend.

Minimum temperature also increased, following the regression equation y=0.0992x−177.43, indicating an annual rise of 0.0992 °C, equivalent to 4 °C over 40 years (Figure 5). The model fit was stronger than for maximum temperature (R^2 = 0.4647). The Mann-Kendall test confirmed a highly significant trend ($p < 0.05$) with a positive S statistic (46.526), and the correlation was moderate to high (Tau = 0.3887), possibly reflecting nighttime warming effects related to urbanization and land use change.

The equivalent study for precipitation led to the results shown below.

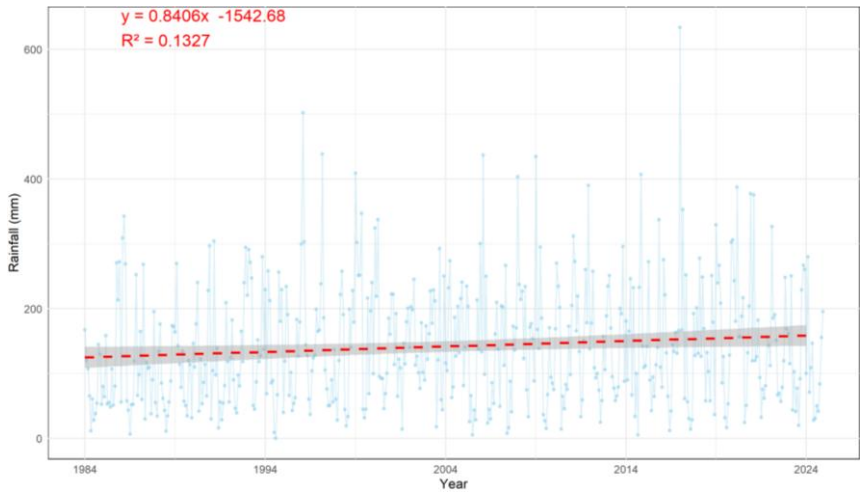

Figure 6. Precipitation time series with annual trend.

Accumulated precipitation showed a slight upward trend, with the regression equation y=0.8406x−1542.68, representing an annual increase of 0.84 mm or 33.6 mm over four decades. However, the model fit was weak ($R^2 = 0.1327$), indicating high interannual variability. The Mann-Kendall test confirmed a significant trend ($p < 0.05$) with a positive S statistic (8.256), although the correlation with time was low (Tau = 0.0684), suggesting that, while increasing, the trend in precipitation is much less pronounced than that of temperature.

Table 1 summarizes the main results obtained from the Mann-Kendall test.

Table 1. Mann-Kendall test. [1]Z is the standard normal statistic, [2]p is the significance level ($p < 0.05$ = significant), [3]S is the Kendall score, and [4]τ (tau) is Kendall's rank correlation coefficient.

Variable	Z[1]	p-value[2]	S[3]	τ[4]
Temperature	[5.9901, 12.774]	<0.001	$[2.18E+04, 4.65E+04]$	[0.183, 0.389]
Rainfall	2.2659	0.0235	8.26E+03	0.068

The methodology identified 16 El Niño and 10 La Niña episodes, classified by duration and intensity. The most notable El Niño events included 1997–1998 (19 months, "extraordinary" intensity), 2015–2016 (16 months, "strong"), and 2023–2024 (14 months, "strong"), all associated with persistent positive thermal anomalies (Table 2).

Table 2. El Niño events (1984-2024). [1]Intensity classification is based on the Coastal El Niño Index (ICEN) and Sea Surface Temperature (SST) anomalies in the Niño 1+2 region.

Onset	Duration (months)	Intensity[1]
December, 1986	13	Moderate
July, 1991	12	Moderate
March, 1993	7	Moderate
November, 1994	3	Weak
March, 1997	19	Extraordinary
March, 2002	3	Weak

Onset	Duration (months)	Intensity[1]
October, 2002	3	Weak
August, 2006	6	Weak
March, 2008	7	Weak
May, 2009	5	Weak
March, 2012	5	Weak
May, 2014	7	Weak
April, 2015	16	Strong
December, 2016	6	Moderate
November, 2018	5	Weak
February, 2023	14	Strong

In contrast, most La Niña episodes were of moderate intensity (7–9 months), except for a "strong" event in 2013 (5 months). These events showed precipitation impacts consistent with historical averages in Pucallpa (Table 3).

Table 3. La Niña events (1984-2024). [1]Intensity classification is based on the Coastal El Niño Index (ICEN) and Sea Surface Temperature (SST) anomalies in the Niño 1+2 region.

Onset	Duration (months)	Intensity[1]
March, 1985	7	Moderate
May, 1988	7	Moderate
April, 1996	4	Moderate
September, 2001	3	Weak
April, 2007	9	Moderate
August, 2010	4	Moderate
April, 2013	5	Strong
November, 2017	5	Weak
November, 2021	9	Weak
September, 2022	3	Weak

During the “extraordinary” 1997–1998 El Niño event, with sea surface temperature (SST) anomalies exceeding +3.0 °C, mean temperature reached 27.5 °C, 1.1 °C above the historical average, peaking at 28.8 °C in January and February 1998 (+2.1 °C above average). In the 2015–2016 “strong” event, with SST anomalies up to +3.0 °C, the mean temperature was 27.3 °C, 0.9 °C above the average, peaking at 28.6 °C in January 2016 (+1.9 °C above average). During the "strong" 2023–2024 event, the mean temperature reached 28.0 °C, 1.6 °C above the historical mean, with a record monthly maximum of 29.8 °C in October 2023 (+3.4 °C above average).

Spearman correlation confirmed a significant positive relationship between El Niño and mean temperatures (rho = 0.15, $p < 0.001$) (Table 4). Let us recall that we use the mean of the interval to calculate the Spearman Coefficient and test.

Table 4. Correlation between climatic variables, El Niño/La Niña, and NDVI. [1]rho = Spearman’s rank correlation coefficient: |rho| < 0.1 (not significant), 0.1–0.3 (weak), 0.3–0.5 (moderate), 0.5–0.7 (strong), ≥0.7 (very strong). [2]Significance levels: ***p < 0.001 (highly significant), **p < 0.01 (very significant), *p < 0.05 (significant), p > 0.05 (not significant).

Variable		El Niño	La Niña	NDVI
Temperature	rho[1]	0.152	0.043	-0.307
	p-value[2]	<0.001***	0.346	<0.001***
Rainfall	rho[1]	-0.079	-0.106	-0.020
	p-value[2]	0.079	<0.05*	0.661

By contrast, the correlation between precipitation and El Niño was negative but not statistically significant (rho = -0.08, p = 0.079), although monthly rainfall during extraordinary El Niño events typically remained below 140 mm (Figure 7).

Figure 7. Climatic variable time series with El Niño event occurrences.

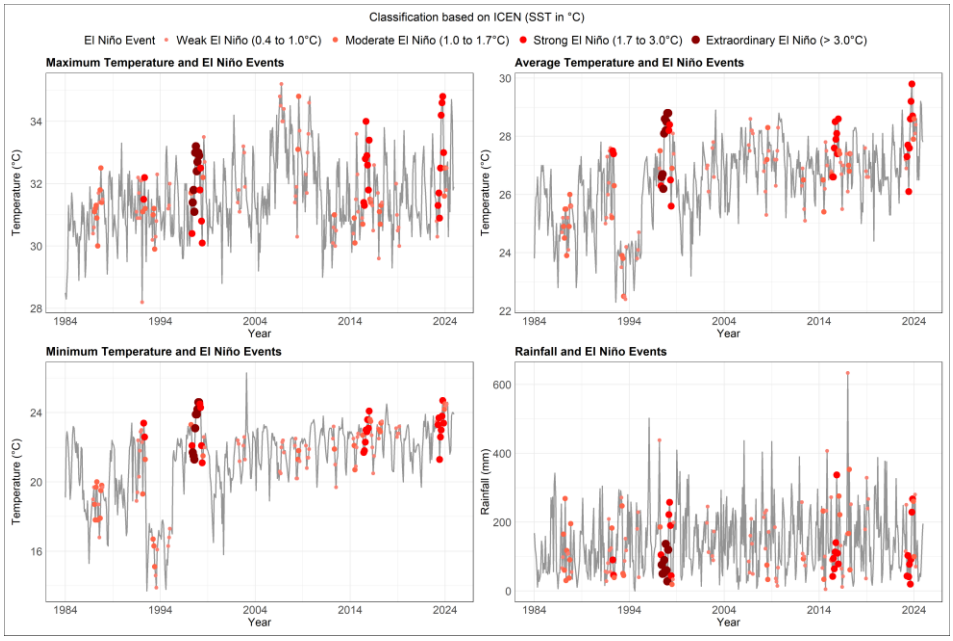

No significant correlations were found between La Niña events and maximum, minimum, or mean temperatures (correlation coefficients < 0.1). However, a weak but statistically significant negative correlation was observed between La Niña and precipitation (rho = -0.11, p = 0.018), suggesting a slight increase in rainfall during these events (Figure 8).

Figure 8. Climatic variable time series with La Niña event occurrences.

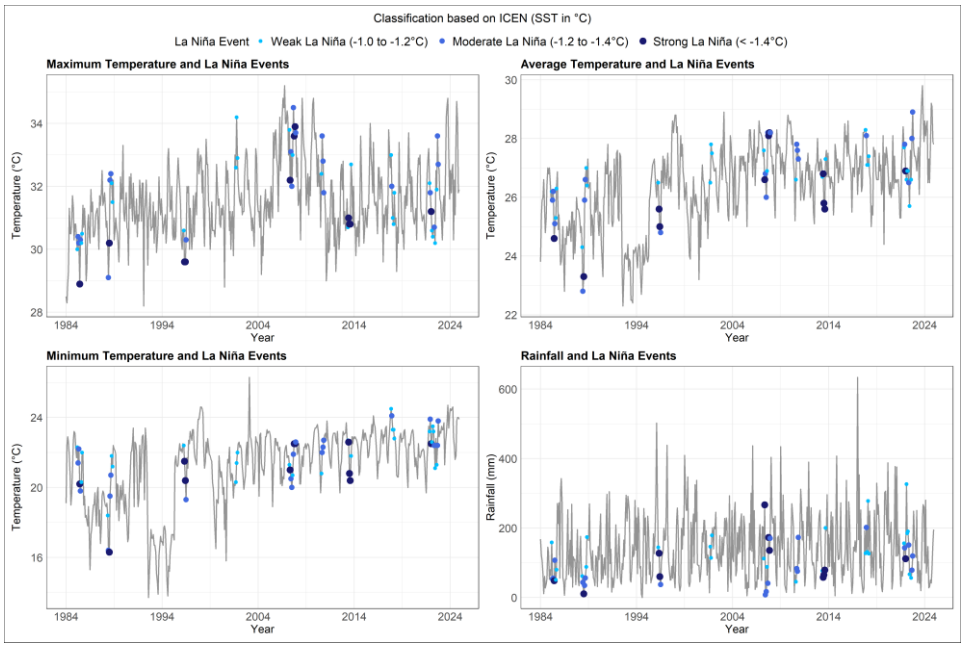

Correlation analysis revealed a negative relationship between NDVI and maximum, mean, and minimum temperatures, with values of rho = -0.31 ($p < 0.001$) for the first two, and rho = -0.165 ($p < 0.001$) for the latter (Table 4). This suggests that vegetation loss is associated with increased thermal values, potentially intensifying the urban heat island effect in peri-urban areas.

Scatterplots showed a descending trend in the fitted linear regressions, with temperature decreasing as NDVI values increased. This pattern was most evident for maximum temperature, reflecting a stronger daytime cooling effect of vegetation, while minimum temperature showed greater dispersion and a shallower slope (Figure 9).

Figure 9. Scatterplots of climatic variables and NDVI.

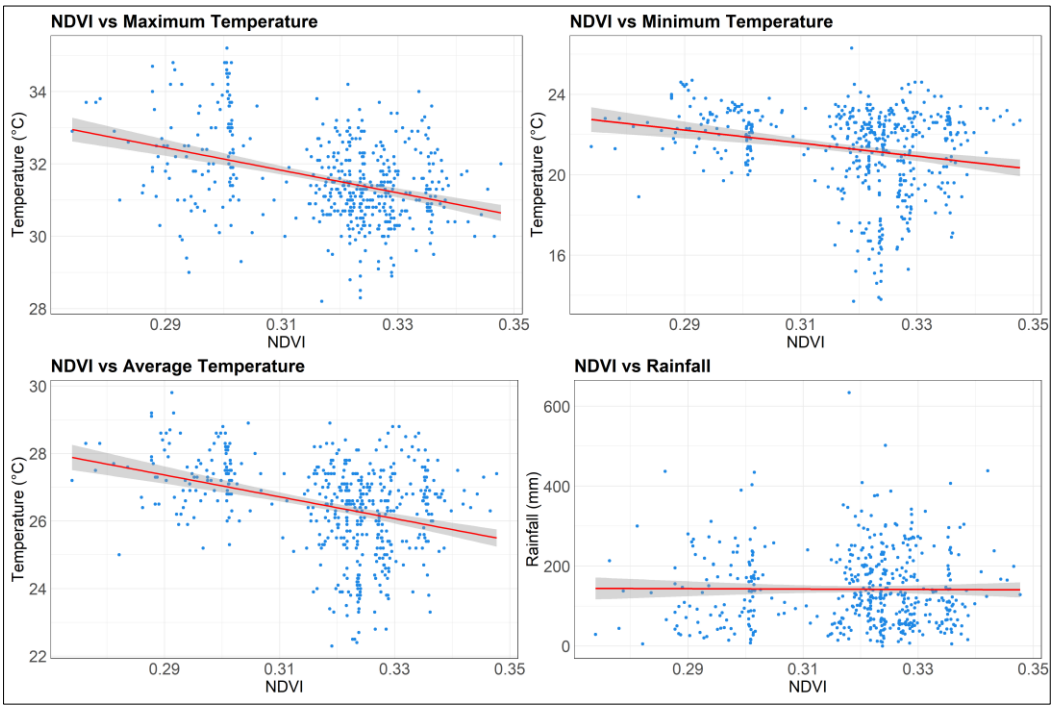

In contrast, the correlation between NDVI and precipitation was nearly zero (rho = -0.02, $p = 0.661$), as reflected in the corresponding plot, where data points were randomly distributed and the regression line was nearly horizontal. This indicates that while vegetation loss influences temperature rise, its impact on accumulated precipitation is minimal or nonexistent.

4. Conclusion

The study revealed a sustained increase in the fluctuation of temperatures in Pucallpa during the analyzed period (1984-2024). A progressive reduction in the Normalized Difference Vegetation Index (NDVI) was observed, showing a negative correlation with rising temperatures and reinforcing the impact of urban expansion. El Niño episodes were associated with significant thermal anomalies, whereas La Niña had negligible effects on temperatures. Precipitation variability exhibited a slight upward trend with high interannual variability, showing no significant relationship with vegetation cover. The research was conducted with interval data of temperature, and Neutrosophic Statistics theory was applied. As in previous studies such as [13], greater accuracy was achieved by considering intervals formed by maximums and minimums than by using a single assessment for each month over the 41 years of the study. This confirms the effectiveness and relevance of using Neutrosophic Statistics in climatic phenomena that are complex by nature.

References

[1] Smarandache, F. Neutrosophic Statistics is an extension of Interval Statistics, while Plithogenic Statistics is the most general form of statistics (second version). Int. J. Neutrosophic Sci. 2022, 19, page range (si está disponible).

[2] Khan, Z.; Krebs, K.L. Enhancing neutrosophic data analysis: A review of neutrosophic measures and applications with Neutrostat. Neutrosophic Sets Syst. 2025, 78, 181-190.

[3] Hanafy, I.M.; Salama, A.A.; Mahfouz, K. Correlation of neutrosophic Data. Int. Ref. J. Eng. Sci. 2012, 1, 39-43.

[4] Gaete, C.C.; Pezoa, V.T.; Escobar, C.R.; Reyes, J.Z. Digital Divide in Latin America: A Multivariate and Neutrosophic Delphi Analysis for Inclusion and Public Policy. Neutrosophic Sets Syst. 2025, 89, 375-390.

[5] Essa, A.K.; Sabbagh, R.; Salama, A.A.; Khalid, H.E.; Aziz, A.A.A.; Mohammed, A.A. An overview of neutrosophic theory in medicine and healthcare. Neutrosophic Sets Syst. 2023, 61, 196-208.

[6] Smarandache, F. Indeterminacy in neutrosophic theories and their applications. Neutrosophic Comput. Mach. Learn. 2025, 39, 1-7.

[7] Woodall, W.H.; Driscoll, A.R.; Montgomery, D.C. A review and perspective on neutrosophic statistical process monitoring methods. IEEE Access 2022, 10, 100456-100462.

[8] Aslam, M.; Arif, O.H.; Sherwani, R.A.K. New diagnosis test under the neutrosophic statistics: an application to diabetic patients. BioMed Res. Int. 2020, 2020, 2086185.

[9] AlAita, A.; Talebi, H.; Aslam, M.; Al Sultan, K. Neutrosophic statistical analysis of split-plot designs. Soft Comput. 2023, 27, 7801-7811.

[10] Macas-Acosta, G.; Márquez-Sánchez, F.; Vergara-Romero, A.; Ricardo, J.E. Analyzing the income-education nexus in ecuador: A neutrosophic statistical approach. Neutrosophic Sets Syst. 2024, 66, 196-203.

[11] Sherwani, R.A.K.; Aslam, M.; Raza, M.A.; Farooq, M.; Abid, M.; Tahir, M. Neutrosophic normal probability distribution—a spine of parametric neutrosophic statistical tests: properties and applications. In Neutrosophic operational research: methods and applications; Publisher: Cham, Switzerland, 2021; pp. 153-169.

[12] Reales Chacón, L.J.; Freire Núñez, J.P.; De la Cruz López, C.A.; García Camacho, V.M.; Silva Guayasamín, L.G.; Ayala, J.G.B. Study of the relationship between moderate intermittent exercise and blood pressure in institutionalized older adult patients, using the neutrosophic correlation coefficient. Neutrosophic Sets Syst. 2024, 71.

[13] Kandemir, H.Ş.; Aral, N.D.; Karakaş, M.; Et, M. Neutrosophic statistical analysis of temperatures of cities in the southeastern Anatolia region of Turkey. Neutrosophic Syst. Appl. 2024, 14, 50-59.

[14] Singh, A.; Kulkarni, H.; Smarandache, F.; Vishwakarma, G.K. Computation of separate ratio and regression estimator under neutrosophic stratified sampling: An application to climate data. J. fuzzy ext. appl. 2024, 5, 605-621.

[15] Coccia, M.; Roshani, S. Evolution of topics and trends in emerging research fields: multiple analyses with entity linking, Mann–Kendall test and burst methods in cloud computing. Scientometrics 2024, 129, 5347-5371.

[16] Nguyen, H.M.; Ouillon, S.; Vu, V.D. Sea level variation and trend analysis by comparing Mann–Kendall test and innovative trend analysis in front of the Red River Delta, Vietnam (1961–2020). Water 2022, 14, 1709.

[17] Baig, M.R.I.; Shahfahad; Naikoo, M.W.; Ansari, A.H.; Ahmad, S.; Rahman, A. Spatio-temporal analysis of precipitation pattern and trend using standardized precipitation index and Mann–Kendall test in coastal Andhra Pradesh. Model. Earth Syst. Environ. 2022, 8, 2733-2752.

[18] Ali Abd Al-Hameed, K. Spearman's correlation coefficient in statistical analysis. Int. J. Nonlinear Anal. Appl. 2022, 13, 3249-3255.

[19] Zhang, L.; Wang, L. Optimization of site investigation program for reliability assessment of undrained slope using Spearman rank correlation coefficient. Comput. Geotech. 2023, 155, 105208.

Received: May 14, 2025. Accepted: July 23, 2025.